Dynamic reconstruction of heterogeneous materials and microstructure evolution

Shaohua Chen,[1] Hechao Li,[2] and Yang Jiao[1,*]
[1]*Materials Science and Engineering, Arizona State University, Tempe, Arizona 85287, USA*
[2]*Mechanical Engineering, Arizona State University, Tempe, Arizona 85287, USA*
(Received 10 June 2015; published 10 August 2015)

Reconstructing heterogeneous materials from limited structural information has been a topic that attracts extensive research efforts and still poses many challenges. The Yeong-Torquato procedure is one of the most popular reconstruction techniques, in which the material reconstruction problem based on a set of spatial correlation functions is formulated as a constrained energy minimization (optimization) problem and solved using simulated annealing [Yeong and Torquato, Phys. Rev. E **57**, 495 (1998)]. The standard two-point correlation function S_2 has been widely used in reconstructions, but can also lead to large structural degeneracy for certain nearly percolating systems. To improve reconstruction accuracy and reduce structural degeneracy, one can successively incorporate additional morphological information (e.g., nonconventional or higher-order correlation functions), which amounts to reshaping the energy landscape to create a deep (local) energy minimum. In this paper, we present a dynamic reconstruction procedure that allows one to use a series of auxiliary S_2 to achieve the same level of accuracy as those incorporating additional nonconventional correlation functions. In particular, instead of randomly sampling the microstructure space as in the simulated annealing scheme, our procedure utilizes a series of auxiliary microstructures that mimic a physical structural evolution process (e.g., grain growth). This amounts to constructing a series auxiliary energy landscapes that bias the convergence of the reconstruction to a favored (local) energy minimum. Moreover, our dynamic procedure can be naturally applied to reconstruct an actual microstructure evolution process. In contrast to commonly used evolution reconstruction approaches that separately generate individual static configurations, our procedure continuously evolves a single microstructure according to a time-dependent correlation function. The utility of our procedure is illustrated by successfully reconstructing nearly percolating hard-sphere packings and particle-reinforced composites as well as the coarsening process in a binary metallic alloy.

DOI: 10.1103/PhysRevE.92.023301 PACS number(s): 02.70.−c, 05.20.−y, 61.43.−j

I. INTRODUCTION

Heterogeneous materials such as composites, alloys, granular materials, and porous media abound in nature and synthetic situations. Successful applications of such materials require accurate assessments and predictions of the effective material properties and their performance under extreme conditions, which in turn rely on the accurate knowledge of the complex material microstructure and quantitative structure-property relations [1–3]. Generating virtual three-dimensional (3D) microstructure is a key step in establishing rigorous structure-property relations. Although certain advanced imaging techniques, such as x-ray tomographic microscopy [4–7], allow one to directly obtain sufficient structural information in a nondestructive manner for 3D material rendition, there are still material systems for which only limited morphological information are available, such as those in x-ray scattering experiments [8,9].

Recently, a variety of material reconstruction methods using limited structural information contained in different statistical morphological descriptors have been developed. Examples of such reconstruction techniques include the Gaussian random field method [10], stochastic reconstruction procedure [11,12], gradient-based method [13], phase recovery method [14], multipoint reconstruction method [15], and raster-path method [16], to name but a few. The structural descriptors utilized in the reconstructions usually arise in rigorous structure-property analysis [17–27] and statistically capture different geometrical and topological features of the material system. Examples include the standard two-point correlation function S_2 [1,2], which gives the probability of finding two specific points in the material phase of interest. The general n-point correlation function S_n provides the probability of finding a specific n-point configuration in the phase of interest. The integrals of S_n are involved in various rigorous bounds [17] and contrast expansions [18,19] of effective material properties. Interested readers are referred to Ref. [2] for a detailed discussion of correlation functions and their properties.

The stochastic reconstruction procedure [11,12], also referred to as the Yeong-Torquato (YT) procedure in literature, is one of the most popular material reconstruction techniques. In principle, the YT procedure allows one to incorporate an arbitrary number of correlation functions of any types into the reconstructions (with increasing computational cost when more correlation functions are used). Specifically, the reconstruction problem is formulated as an energy minimization problem, with the energy E defined for a trial microstructure as the difference between the target and simulated correlation functions. The space of trial microstructure (i.e., microstructure space) is then randomly searched to find one that minimizes E (with an ideal minimum of zero). This is done by evolving an initial random trial microstructure using the simulated annealing procedure such that in the end the trial microstructure possesses an energy value smaller than a prescribed tolerance (see Sec. III for algorithmic details). The YT procedure is very flexible and versatile in dealing with different material systems. However,

*yang.jiao.2@asu.edu

due to its stochastic nature, a large number of intermediate trial microstructures need to be generated and analyzed, which makes it computationally intensive. Several improved implementations of the YT procedure have been devised to improve efficiency [28–32], preserve isotropy [33–35], and handle anisotropic materials [36–38].

Although the two-point correlation function S_2 is widely used for reconstructing a wide class of material systems, it generally does not contain sufficient morphological information to uniquely determine a microstructure [39,40]. Thus, reconstructions using S_2 alone can lead to large structural degeneracy (i.e., a large number of distinct microstructures compatible with the specified correlation function) [40], especially for nearly percolating systems in which the volume fraction ϕ of one of the phases is close to the critical value ϕ_c beyond which a system-spanning cluster of that phase emerges [2,3]. To reduce structural degeneracy and increase reconstruction accuracy, a variety of nonstandard correlation functions, such as the two-point cluster function C_2 providing topological connectedness information [21,22] and surface-surface correlation function F_{ss} providing interface information [23], have also been incorporated into the YT procedure [30] (see definitions in Sec. II). It has been shown that these nonstandard correlation functions contain higher-order structural information encoded in S_n and thus, incorporating them in the reconstruction can significantly reduce the number of compatible microstructures [30]. This amounts to reshaping the energy landscape (defined over all possible microstructures) to create a deep (local) energy minimum with a wide and smooth basin, which has a very high probability of being identified by the random microstructure search (see Fig. 1).

In this paper, we present a dynamic reconstruction procedure within the Yeong-Torquato framework that allows one to use a series of auxiliary S_2 to achieve the same level of accuracy as those incorporating additional nonconventional correlation functions. In particular, instead of randomly sampling the microstructure space as in the standard YT simulated annealing scheme, our procedure utilizes a series of auxiliary microstructures that mimic a physical structural evolution process (e.g., grain growth). Such auxiliary microstructures are obtained, e.g., by successive isotropic erosion of the original target microstructure [41,42]. For each auxiliary microstructure, the associated S_2 is computed and the reconstruction process proceeds by growing as well as successively evolving the morphology of the target phase according the series of target S_2s. This also amounts to constructing a series auxiliary energy landscapes, one associated with each S_2 in the series, that bias the convergence of the reconstruction to a favored (local) energy minimum (see Fig. 1). We note that our procedure is different from a recently developed dilation and erosion method [41,42], which transforms topologically complex structures to simpler ones and utilizes appropriate topological descriptors such as C_2 for accurate reconstructions of the original system.

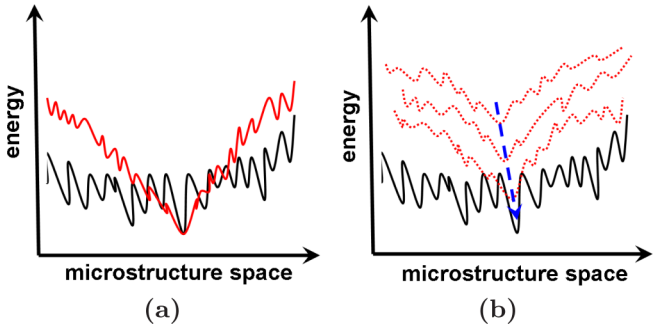

FIG. 1. (Color online) Schematic illustration of different modifications of energy landscape to improve convergence for different reconstruction methods within the Yeong-Torquato framework. The original funnel energy landscape associated with S_2 is illustrated by the black curve in both panels. (a) Incorporating additional correlation functions amounts to reshaping the energy landscape to create a deep (local) energy minimum with a wide and smooth basin (red curves or dark gray curves in print version). (b) The dynamic reconstruction utilizes a series of auxiliary energy landscapes (dashed red curves or dark gray curves in print version) to bias the convergence of reconstruction to the favor microstructure (illustrated by the dashed blue arrow or light gray arrow in print version).

Moreover, the dynamic reconstruction procedure can be naturally applied to reconstruct a microstructure evolution process. In this case, the series of S_2 characterize snapshots of the material microstructure at successive time points during the evolution and, thus, can be considered as a single time-dependent correlation function evaluated at different time points. In contrast to commonly used evolution reconstruction approaches that separately generate individual static configurations, our procedure continuously evolves a single microstructure according to a time-dependent correlation function. The utility of our procedure is illustrated by successfully reconstructing nearly percolating hard-sphere packings and particle-reinforced composites as well as the coarsening process of a binary metallic alloy.

The rest of the paper is organized as follows: In Sec. II, we provide definitions of various correlation functions employed in this paper. In Sec. III, we present the dynamic reconstruction procedure in detail. In Secs. IV and V, we respectively apply our procedure to successively reconstruct nearly percolating systems and microstructure evolution based on two-point correlation functions alone. In Sec. VI, we make concluding remarks.

II. STATISTICAL MORPHOLOGICAL DESCRIPTORS

A. *n*-point correlation function

In general, the microstructure of a heterogeneous material can be uniquely determined by specifying the indicator functions associated with all of the individual phases of the material [1,2]. Without loss of generality, we focus on two-phase materials (binary medium) in this work. We note that the generalization of the subsequent discussion to a multiple-phase system is straightforward.

Consider a statistically homogeneous material M occupying the region $\mathcal{V}$ in the d-dimensional Euclidean space $\mathbb{R}^d$ ($d = 1,2,3$), which is partitioned into two disjoint phases: phase 1, regions $\mathcal{V}_1$ of volume fraction ϕ_1 and phase 2, regions $\mathcal{V}_2$ of volume fraction ϕ_2. It is obvious that $\mathcal{V}_1 \cup \mathcal{V}_2 = \mathcal{V}$ and $\mathcal{V}_1 \cap \mathcal{V}_2 = \mathbf{0}$. The indicator function $\mathcal{I}^{(i)}(\mathbf{x})$ of phase i is given

by

$$\mathcal{I}^{(i)}(\mathbf{x}) = \begin{cases} 1 & \mathbf{x} \in \mathcal{V}_i, \\ 0 & \mathbf{x} \in \bar{\mathcal{V}}_i, \end{cases} \tag{1}$$

for $i = 1,2$ with $\mathcal{V}_i \cup \bar{\mathcal{V}}_i = \mathcal{V}$ and

$$\mathcal{I}^{(1)}(\mathbf{x}) + \mathcal{I}^{(2)}(\mathbf{x}) = 1. \tag{2}$$

The n-point correlation function $S_n^{(i)}$ for phase i is defined as follows:

$$S_n^{(i)}(\mathbf{x}_1,\mathbf{x}_2,\ldots,\mathbf{x}_n,) = \langle \mathcal{I}^{(i)}(\mathbf{x}_1)\mathcal{I}^{(i)}(\mathbf{x}_2)\ldots\mathcal{I}^{(i)}(\mathbf{x}_n)\rangle, \tag{3}$$

where the angular brackets $\langle\ldots\rangle$ denote ensemble averaging over independent realizations of the medium. The two-point correlation function $S_2^{(i)}$ for phase i is defined by

$$S_2^{(i)}(\mathbf{x}_1,\mathbf{x}_2) = \langle \mathcal{I}^{(i)}(\mathbf{x}_1)\mathcal{I}^{(i)}(\mathbf{x}_2)\rangle. \tag{4}$$

For a statistically homogeneous medium, $S_2^{(i)}$ is a function of the relative displacements of point pairs, i.e.,

$$S_2^{(i)}(\mathbf{x}_1,\mathbf{x}_2) = S_2^{(i)}(\mathbf{x}_2 - \mathbf{x}_1) = S_2^{(i)}(\mathbf{r}), \tag{5}$$

where $\mathbf{r} = \mathbf{x}_2 - \mathbf{x}_1$. If the medium is also statistically isotropic, $S_2^{(i)}$ is a radial function, depending on the separation distances of point pairs only, i.e.,

$$S_2^{(i)}(\mathbf{x}_1,\mathbf{x}_2) = S_2^{(i)}(|\mathbf{r}|) = S_2^{(i)}(r). \tag{6}$$

Interested readers are referred to Ref. [2] for a detailed discussion of $S_2^{(i)}$ and other higher-order $S_n^{(i)}$. Henceforth, we will drop the superscript i in $S_2^{(i)}$ for simplicity. Without further elaboration, S_2 is always the two-point correlation function of the phase of interest.

B. Surface correlation functions

The surface correlation functions contain information about the random interface in a heterogeneous system [23]. Since such statistics arise in and are of basic importance in the trapping and flow problems, it is conventional in that context to let phase 1 denote the fluid or void phase, and phase 2 denote the solid phase. The simplest surface correlation function is the specific surface $s(\mathbf{x})$ at point $\mathbf{x}$, which gives the interface per unit volume, i.e.,

$$s(\mathbf{x}) = \langle \mathcal{M}(\mathbf{x})\rangle, \tag{7}$$

where $\mathcal{M}(\mathbf{x})$ is the interface indicator function defined as the absolute gradient of the phase indicator function, i.e.,

$$\mathcal{M}(\mathbf{x}) = |\bigtriangledown\, \mathcal{L}(\mathbf{x})|. \tag{8}$$

We note that for statistically homogeneous material, the specific surface is a constant everywhere and thus, is simply denoted by s.

The two-point surface correlation functions for a general heterogeneous material are defined by

$$F_{ss}(\mathbf{x}_1,\mathbf{x}_2) = \langle \mathcal{M}(\mathbf{x}_1)\mathcal{M}(\mathbf{x}_2)\rangle, \tag{9}$$

and

$$F_{sv}(\mathbf{x}_1,\mathbf{x}_2) = \langle \mathcal{M}(\mathbf{x}_1)\mathcal{L}(\mathbf{x}_2)\rangle, \tag{10}$$

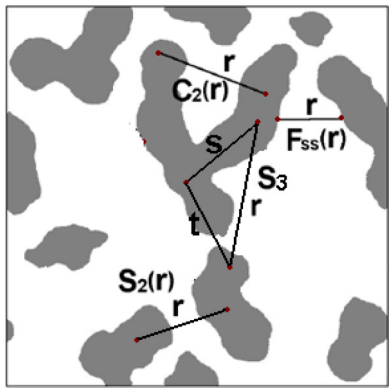

FIG. 2. (Color online) Schematic illustration of the probability interpretation of the correlation functions employed in this work. The line segments (two-point configurations) and triangles (three-point configurations) illustrate the events that contribute to the corresponding correlation functions.

which are respectively called the surface-surface and surface-void correlation functions [2,23]. For statistically homogeneous and isotropic materials, the functions F_{ss} and F_{sv} only depend on the scalar distance $r = |\mathbf{x}_1 - \mathbf{x}_2|$. We note that unlike S_n, the surface correlation functions do not have a direct probability interpretation, since the probability of finding a point exactly falling on the the interface is always zero. Instead, they can be associated with the probability of finding points in the dilated interface region with thickness δ in the limit $\delta \to 0$ [30] (see Fig. 2).

C. Two-point cluster function

The two-point cluster correlation function $C_2(\mathbf{x}_1,\mathbf{x}_2)$ gives the probability that two randomly selected points x_1 and x_2 fall into the same cluster of the phase of interest [21,22] (see Fig. 2). For statistically homogeneous and isotropic materials, C_2 depends only on the relative distance r between the two points. It contains complete clustering information of the phases, which has been shown to have dramatic effects on the material's physical properties [2,3]. However, unlike S_2 and the surface correlation functions, the cluster function generally cannot be obtained from lower-dimensional cuts (e.g., 2D slices) of a 3D microstructure, which may not contain correct connectedness information of the actual 3D system.

It has been shown that C_2 is related to S_2 via the following equation [22]

$$S_2(r) = C_2(r) + D_2(r), \tag{11}$$

where $D_2(r)$ measures the probability that two points separated by r fall into different clusters of the phase of interest. In other words, C_2 is the connectedness contribution to the standard two-point correlation function S_2. For microstructures with well-defined inclusion, $C_2(r)$ of the inclusions is a short-ranged function that rapidly decays to zero as r approaches the largest linear size of the inclusions. We note that although C_2 is a two-point quantity, it has been shown to encode higher-order structural information, which makes it a highly sensitive statistical descriptor over and above S_2 [30].

D. Computing correlation functions from images

The aforementioned correlation functions can be effectively computed from given digital images of a material, in which the microstructure is represented as a 2D (or 3D) array of pixels (or voxels). In such arrays, each entry indicates the local state (e.g., phase) of that pixel. For a binary system, the array is simply a collection of black and white pixels on a regular lattice. The probabilistic interpretation of the correlation functions enable us here to develop a general sampling method for reconstruction of statistically homogeneous and isotropic digitized textures based on the lattice-gas formalism, which is introduced in Ref. [34] and generalized in Ref. [30]. In the generalized formalism, pixels with different values (occupying the lattice sites) correspond to distinct local states and pixels with the same value are considered to be molecules of the same gas species [34]. The correlation functions of interest can be obtained by binning the separation distances between the selected pairs of molecules from particular species.

For example, the standard two-point correlation function S_2 can be computed as follows:

$$S_2(r) = N_P(r)/N_S(r), \tag{12}$$

where $N_S(r)$ is the number of lattice-site separation distances of length r and $N_P(r)$ gives he number of molecule-pair separation distances of length r. The two-point cluster function C_2 is given by

$$C_2(r) = \sum_i N_P^i(r)/N_S(r), \tag{13}$$

where $N_P^i(r)$ denotes the pair distances of length r between the molecules within the same cluster i. The surface-surface correlation function F_{ss} can be obtained by

$$F_{ss}(r) = N^{ss}(r)/N_S(r), \tag{14}$$

where $N^{ss}(r)$ gives the number of distances between two surface molecules with length r. Additional details about this method are provided in Ref. [30].

III. DYNAMIC RECONSTRUCTION METHOD

A. Yeong-Torquato procedure

Our dynamic reconstruction procedure is developed within the Yeong-Torquato (YT) stochastic reconstruction framework [11,12], in which an initial random microstructure is evolved to minimize an energy function that measures the difference between target correlation functions and those of the simulated microstructure. As discussed in Sec. I, there are many other different microstructure reconstruction procedures [10,14–16]. However, the YT procedure incorporates energy-driven microstructure evolution, which can be naturally generalized to derive the dynamic reconstruction procedure.

In the YT procedure, the reconstruction problem is formulated as an energy minimization problem, with the energy functional E defined as follows

$$E = \sum_r \sum_\alpha \left[f_n^\alpha(r) - \widehat{f_n^\alpha}(r) \right]^2, \tag{15}$$

where $\widehat{f_n^\alpha}(r)$ is a target correlation function of type α and $f_n^\alpha(r)$ is the corresponding function associated with a trial microstructure. The simulated annealing method [43] is usually employed to solve the aforementioned minimization problem. Specifically, starting from an initial trial microstructure (i.e., old microstructure), which contains a fixed number of voxels for each phase consistent with the volume fraction of that phase, two randomly selected voxels associated with different phases are exchanged to generate a new trial microstructure. Relevant correlation functions are sampled from the new trial microstructure and the associated energy is evaluated, which determines whether the new trial microstructure should be accepted or not via the probability:

$$p_{acc} = \min\{\exp(-\Delta E/T), 1\}, \tag{16}$$

where ΔE is the energy difference between the new and old trial microstructure and T is a virtual temperature T that is chosen to be initially high and slowly decreases according to a cooling schedule [11,12]. An appropriate cooling schedule reduces the chances that the system gets stuck in a shallow local energy minimum. In practice, a power-law schedule $T(n) = \gamma^n T_0$ is usually employed, where T_0 is the initial temperature, n is the cooling stage and $\gamma \in (0,1)$ is the cooling factor ($\gamma = 0.98$ is used here). The simulation is terminated when E is smaller than a prescribed tolerance (e.g., 10^{-6} in this case). Generally, a large number of trial microstructures need to be searched to generate a successful reconstruction. Therefore, highly efficient sampling methods [30,33,34] are used that enable one to rapidly obtain the prescribed correlation functions of a new microstructure by updating the corresponding functions associated with the old microstructure, instead of completely recomputing the functions. The readers are referred to Ref. [30] for details of the efficient correlation function update schemes.

B. Dynamic reconstruction

In the original YT scheme, the microstructure space is randomly sampled and thus, the evolution of the trial microstructure during the reconstruction is not associated with a physical process. In addition, the convergence of the reconstruction strongly depends on the energy landscape defined over the microstructure space [cf. Eq. (15)]. As discussed in Sec. I, for certain nearly percolating systems (e.g., dense particle packings), the energy landscape associated with the reconstruction using $S_2(r)$ alone is very rough and contains many local minima, which usually lead to large structural degeneracy and inaccurate reconstructions. For example, in a typical reconstructed structure, the degree of clustering is significantly overestimated and the particle phase, which is supposed to be disconnected, usually percolates and forms a system spanning cluster [39,40]. One approach to reduce structural degeneracy is to incorporate additional correlation functions such as C_2 and F_{ss}, which reshape the energy landscape to create a deep (local) energy minimum with a wide and smooth basin of attraction. Such a minimum is usually associated with a high probability being visited and selected by the random microstructure research.

The dynamic reconstruction procedure we devise here uses auxiliary energy landscapes to bias the microstructure evolution towards a favored reconstruction. This allows one to use a series of auxiliary S_2 to achieve the same level

of reconstruction accuracy as those incorporating additional nonconventional correlation functions. It works as follows: Given a target digitized two-phase microstructure (2D or 3D) possessing a volume fraction $\phi^{(n)}$ for the phase of interest, say phase 1, the associated two-point correlation function $S_2^{(n)}(r)$ is computed. Then an erosion operation is applied to the microstructure, which is described in detail in the subsequent section. The erosion operation results in a reduced volume fraction of phase 1, i.e., $\phi^{(n-1)}$ and the associated two-point correlation function $S_2^{(n-1)}(r)$ is computed. This process is repeated n times until the morphology of phase 1 consists of well-separated compact particles with a very low volume fraction $\phi^{(0)}$, which results in a series of correlation functions $\{S_2^{(0)}(r), S_2^{(1)}(r), \ldots, S_2^{(n)}(r)\}$.

To reconstruct the original system, instead of directly using $\hat{S}_2$ of the target microstructure, we start from $S_2^{(0)}$ associated with the eroded system possessing the lowest volume fraction $\phi^{(0)}$. A corresponding microstructure is then reconstructed using the YT procedure, which has been shown to be highly efficient in generating accurate reconstruction at such low ϕ. The reconstructed microstructure is then used as the initial configuration for reconstructing the structure with $\phi^{(1)}$ from $S_2^{(1)}$. Specifically, a new trial microstructure is generated from the current configuration by adding pixels of phase 1 to randomly selected locations at the two-phase interface to increase the volume fraction from $\phi^{(0)}$ to $\phi^{(1)}$. Then YT procedure is applied in which only surface pixels are randomly selected and displaced on the surface. The resulting new trial microstructure is accepted with a probability specified by Eq. (16) and simulated annealing is used to evolve the system.

We note that this approach is distinct from a conventional YT procedure in two aspects: (i) a favored initial configuration instead of a random one is used, which is already in the basin associated with an energy minimum; (ii) more efficient evolution kinetics that only involves displacing surface pixels is employed. This corresponds to evolve the energy-minimal configuration $\mathcal{M}^{(k)}$ associated with $S_2^{(k)}$ to the nearest energy-minimal configuration $\mathcal{M}^{(k+1)}$ in the energy landscape associated with $S_2^{(k+1)}$ via surface optimization. This process is repeated to successively generate a series of auxiliary microstructures $\mathcal{M}^{(k)}$, $\mathcal{M}^{(k+1)}$, ..., $\mathcal{M}^{(n)}$ in order to finally accurately reconstruct the original microstructure $\hat{\mathcal{M}}$. It can be seen that during the entire reconstruction process, a series of auxiliary energy landscapes are constructed, each associated with a $S_2^{(k)}$ $(k = 0, 1, \ldots, n)$. These auxiliary landscapes successively bias the evolution path of the trial microstructure to improve the convergence of the reconstruction (see Fig. 1). Our procedure is also different from a recently developed dilation and erosion method [41,42], which transforms a topologically complex structure to simpler one, and utilizes appropriate topological descriptors such as C_2 for accurate reconstructions of the original system. No auxiliary landscapes are used in the dilation and erosion approach.

Moreover, the dynamic reconstruction procedure is readily applicable to reconstruction of a microstructure evolution process. In this case, the series $\{S_2^{(0)}(r), S_2^{(1)}(r), \ldots, S_2^{(n)}(r)\}$ characterizes snapshots of the materials at successive time points during the evolution and thus, can be considered as a single time-dependent correlation function evaluated at different time points. This is to be distinguished from the series of auxiliary S_2 obtained from the erosion process, for which the inverse reconstruction from a low-density initial configuration only mimics a physical evolution process. In contrast to commonly used evolution reconstruction approaches that separately generate individual static configurations, our procedure continuously evolves a single microstructure according to a time-dependent correlation function.

C. Generating serial S_2 using erosion operation

As discussed in the previous section, an erosion operation is employed to generate auxiliary microstructures, from which the auxiliary correlation functions $\{S_2^{(0)}(r), S_2^{(1)}(r), \ldots, S_2^{(n)}(r)\}$ are computed. Specifically, the operation successively removes surface layers of the phase 1 and convert the associated pixels into phase 2. (The surface layer of phase 1 is defined as a layer of pixel that has at least one neighbor pixel of phase 2). We now describe the erosion procedure devised for particulate microstructure in detail.

Our erosion operation mimics a physical erosion process, see Fig. 3. For example, for material in a erosive environment, the erosion rates at different locations are different and depend on the local morphology as well as the environment. Generally speaking, geometrical singular regions with more exposure to the environment such as corners and protrusion are more easily eroded out. To achieve this in our simulated erosion process, we first examine the target microstructure and obtain the centers of mass (COM) of each individual grains. Then we place equal-sized circles (or spheres in 3D) centered at COMs to enclose the grains in the system. The radius of circles is initially large and successively decreased until the circles intersect with the grains. The regions of grains that are not enclosed by the circles are removed, and the reduced density $\phi^{(k)}$ as well as the associated correlation function $S_2^{(k)}$ is computed, where k corresponds to this erosion stage. This process is repeated until the morphology of the phase of interest consists of well-separated compact particles with a very low volume fraction $\phi^{(0)}$. Generally, our erosion operation reduces geometrical singularities (e.g., sharp corners, elongated protrusions, etc.) as well as size dispersity in the microstructure, leading to an easy-to-reconstruct configuration

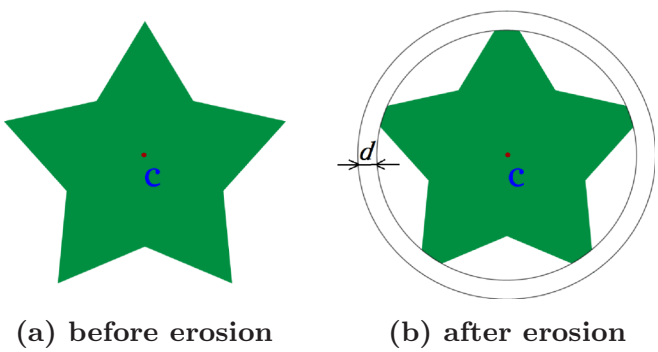

FIG. 3. (Color online) A schematic illustration of erosion operation. (a) shows the target grain, whose center of mass is denoted by "c". (b) shows the grain morphology after an erosion operation, where d is the change of the radius of the circle enclosing the grain.

via the YT procedure. For example, at a certain stage, all the grains could become equal-sized circles (or spheres in 3D) with a very low volume fraction, which are easily reconstructed via the YT procedure. This is to be distinguished from the erosion method used in Refs. [41,42], in which erosion occurs along the direction normal to the surface and thus, preserves the geometrical singularities and particle size distribution in the eroded microstructures.

IV. RECONSTRUCTING NEARLY PERCOLATING MICROSTRUCTURE

In this section, we apply the dynamic reconstruction procedure to generate virtual microstructures of 3D binary heterogeneous materials in which one of the phases is nearly percolating. Specifically, two systems are considered here: a packing of equal-sized hard spheres [44] and a SiC-particle reinforced Al-matrix composite [45] with a particle-phase volume fraction close to the corresponding percolation thresholds. Previous studies have shown that the standard YT reconstruction using S_2 alone significantly overestimates the degree of clustering of the particle phase in such systems. In the following, we will show that our procedure not only correctly reproduces the connectedness of the particle phase but also reasonably resolve the shape and size distribution for the SiC particles.

A. Packing of equal-sized hard spheres

We first consider a packing of equal-sized hard spheres with packing fraction (i.e., volume fraction of the particle phase) $\phi = 0.283$ (see Fig. 4). The packing is generated by compressing a low-density initial configuration of $N = 199$ spheres via the adaptive-shrinking-cell method [46].

The erosion operation described in Sec. III C is employed to generate a series of auxiliary structures. Specifically, the spheres are successively shrunk until each sphere is represented by a single voxel. The resulting series of correlation functions $S_2^{(j)}$ are computed and employed to successively reconstruct the auxiliary structures, see Fig. 5. The final reconstruction is shown in Fig. 6(a). It can be clearly seen that well-separated equal-sized spherical particles are produced. This is to be contrasted with the S_2-alone reconstruction using the standard YT procedure, in which the particle phase is connected as shown in Fig. 6(b). To quantitatively ascertain the accuracy of the dynamic reconstruction, the two-point cluster function C_2 and surface-surface correlation function F_{ss} computed from both the target and reconstructed structures are compared in Fig. 6(c). In the case of dynamic

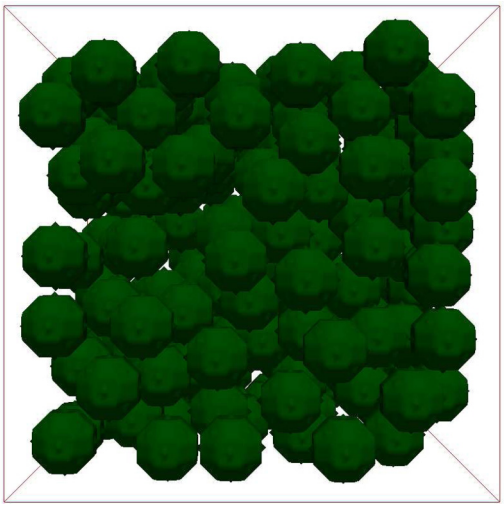

FIG. 4. (Color online) A packing of $N = 199$ equal-sized hard spheres with packing fraction $\phi = 0.283$.

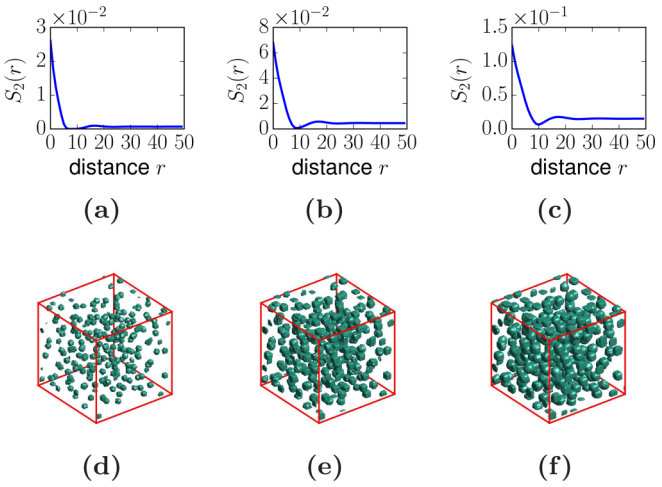

FIG. 5. (Color online) Dynamic reconstruction of a dense hard-sphere packing system. Auxiliary structures (d)–(f) are successively reconstructed from the associated correlation functions (a)–(c) based on previously reconstructed structures as favored initial configurations.

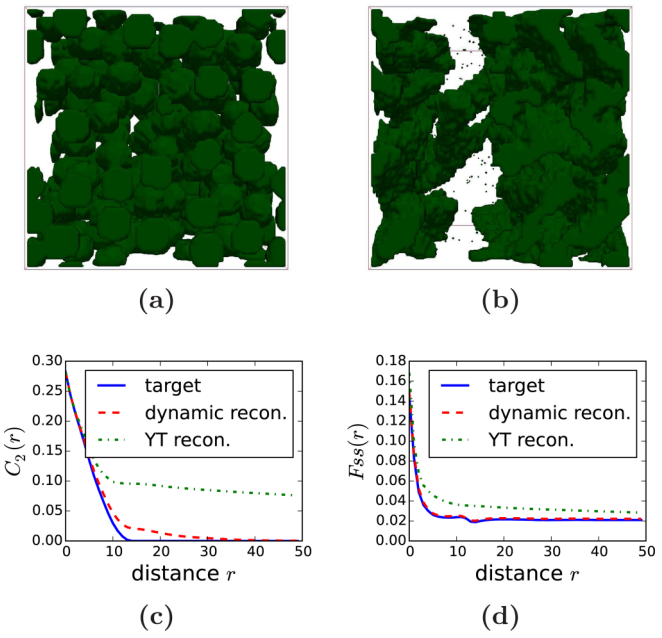

FIG. 6. (Color online) Reconstructed systems based on S_2 alone. (a) Dynamics reconstruction. (b) Standard YT reconstruction. Comparison of (c) C_2 and (d) F_{ss} computed from the target and reconstructed microstructures.

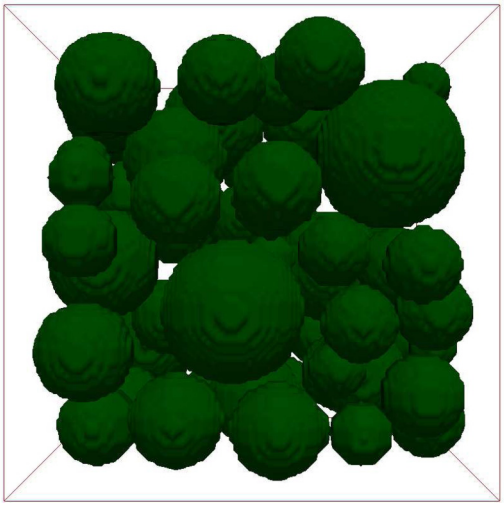

FIG. 7. (Color online) A SiC-particle reinforced Al-matrix composite material with particle volume fraction $\phi = 0.31$. Only the particle is shown and the matrix is transparent. The linear size of the system is 200 μm. The whole system is digitized into $100 \times 100 \times 100$ voxels.

reconstruction, the corresponding functions match very well with one another, indicating the high accuracy of the dynamic reconstruction. It can be clearly seen that the YT procedure significantly overestimates the clustering in the reconstruction, as shown by the long-range C_2 in Fig. 6(c). In addition, the YT reconstruction also overestimates the number of surface voxels, as indicated by the larger values of F_{ss}, compared to the target function as shown in Fig. 6(d).

B. SiC/Al composite

Figure 7 shows a model microstructure of SiC-particle reinforced Al-matrix composite [45] with particle volume fraction $\phi = 0.31$. It can be seen that the isotropic SiC particles possess a wide size distribution. Although the particle volume fraction is close to the percolation threshold, the particle phase is still disconnected, which makes the system very difficult to reconstruct using the standard YT procedure based on S_2 alone.

The erosion operation described in Sec. III C is employed to generate a series of auxiliary structures. Specifically, the SiC particles are successively shrunk until the smallest particle is represented by a few voxels. The resulting correlation functions $S_2^{(j)}$ are computed and employed to successively reconstruct the auxiliary structures, see Fig. 8. The final reconstruction is shown in Fig. 9(a). It can be clearly seen that the size distribution of SiC particles are very well resolved in the reconstruction. This is also quantitatively indicated from the comparison of the two-point cluster function C_2 and surface-surface correlation function F_{ss} computed from the target and the reconstruction, as shown in Fig. 9(c). Also shown is the reconstructed system using the standard YT procedure from S_2 alone [Fig. 9(b)], in which the clustering of the particle phase is again significantly overestimated.

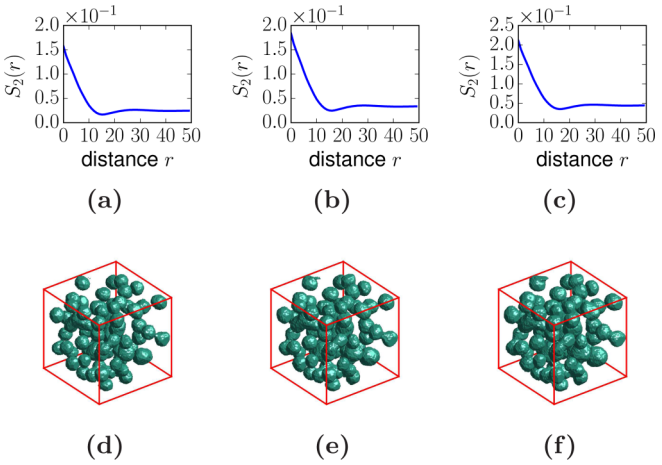

FIG. 8. (Color online) Dynamic reconstruction of the SiC/Al composite system. (d)–(f) Auxiliary structures are successively reconstructed from the (a)–(c) associated correlation functions based on previously reconstructed structures as favored initial configurations.

V. RECONSTRUCTING MICROSTRUCTURE EVOLUTION

In this section, we apply the dynamic reconstruction procedure to reproduce the microstructure coarsening process in a binary lead/tin alloy aged at 448 K up to 216 hours [35]. It has been shown that the scaled autocorrelation function of this system, i.e.,

$$f(r) = \frac{S_2(r) - \phi^2}{\phi(1-\phi)}, \tag{17}$$

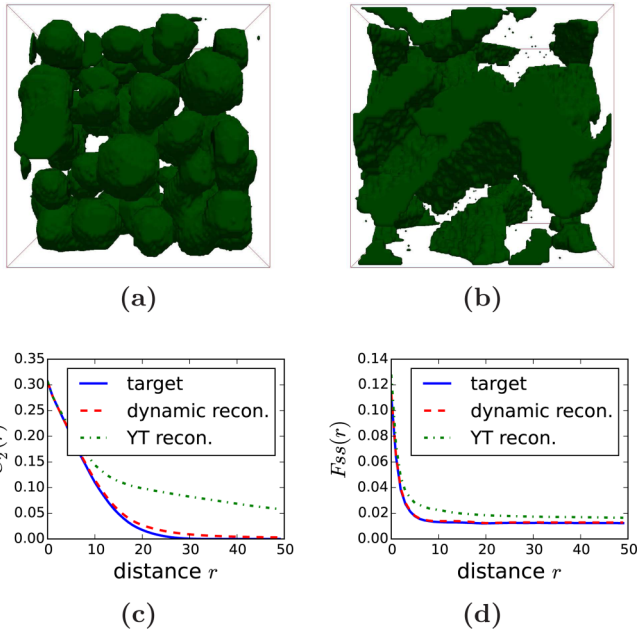

FIG. 9. (Color online) Reconstructed systems based on S_2 alone. (a) Dynamics reconstruction. (b) Standard YT reconstruction. Comparison of (c) C_2 and (d) F_{ss} computed from the target and reconstructed microstructures.

which is same for both the Pb-rich and Sn-rich phases, can be approximated via the following expression [35]

$$f(r;t) = \exp[-ar/\lambda(t)]\cos[\pi r/\lambda(t) + b]/\cos(b), \quad (18)$$

where $a = 3.5$ and $b = 0.60$ are dimensionless fitting parameters depending on the aging temperature and Pb composition and

$$\lambda(t) = \left[\lambda_0^3 + \left(\lambda_f^3 - \lambda_0^3\right)\frac{t}{t_f}\right]^{1/3}, \quad (19)$$

where λ_0 and λ_f are respectively the length scale in the as-processed and final aged microstructures, and t_f is the associated time of aging.

To reconstruct the coarsening process, the two-point correlation function S_2 of the Pb-rich phase is computed at different time points during the evolution, see Fig. 10(a). The dynamic reconstruction is employed to successively evolve the microstructure according to the series of S_2, see Fig. 10(b). We note that the coarsening process is diffusion controlled, thus, the phase morphological changes occur through the two-phase interface. This makes the surface-evolution kinetics utilized in our reconstruction procedure naturally mimics the actual physical evolution process, and therefore highly efficient in reconstructing the structural evolution.

To quantitatively ascertain the quality of the reconstruction, the reconstructed system at selected time points are compared both visually and qualitatively to the 2D optical micrographs of the alloy at the corresponding time points during the aging experiment, see the upper panels of Fig. 11. Figures 11(b) and 11(c) respectively show the two-point cluster function C_2 and surface-surface correlation function F_{ss} computed from the 2D micrographs and 2D slices of the reconstructed alloy structures. The excellent agreement between the reconstructed and experimental correlation functions clearly indicates the accuracy of the dynamic reconstruction in reproducing the entire microstructure evolution process.

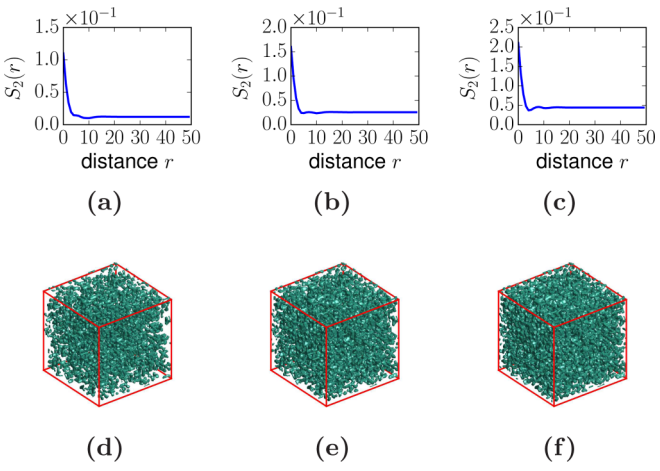

FIG. 10. (Color online) Reconstruction of the coarsening process in a lead/tin alloy from a time-dependent correlation function. (a)–(c) S_2 at different time points during the evolution (i.e., respectively 12, 24, and 48 hours after annealing starts). (d)–(f) The associated microstructures generated using the dynamic reconstruction in which only the Pb-rich phase is shown. The coarsening of the phase is apparent. The linear size of the system is 250 μm. The total annealing time for the alloy is 216 hours.

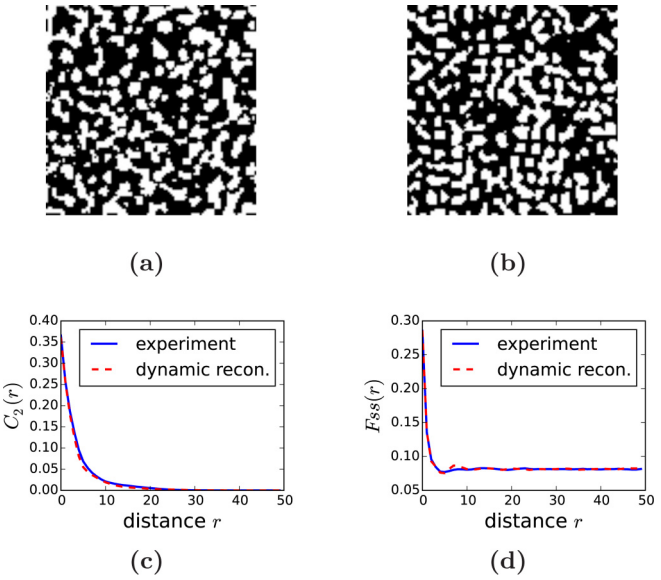

FIG. 11. (Color online) Top: Comparison of (a) a 2D optical micrograph of the alloy at 36 hours after annealing starts and (b) a corresponding 2D slice of the reconstructed structure at the same time point. Bottom: Comparison of the two-point cluster functions (c) C_2 and the surface-surface correlation function (d) F_{ss} for the experimental and reconstructed systems.

VI. CONCLUSIONS AND DISCUSSIONS

In this paper, we have presented a dynamic reconstruction procedure that allows one to use a series of auxiliary S_2 to accurately reconstruct heterogeneous materials in which one of the phases is nearly percolating. Such systems are extremely difficult to reconstruct using the standard YT procedure, which usually significantly overestimates the degree of clustering unless additional nonconventional correlation functions containing appropriate topological information are incorporated. Different from the YT scheme in which the microstructure space is randomly sampled, our procedure utilizes a series of auxiliary energy landscapes and surface-evolution kinetics to bias the microstructure evolution path and improve the convergence of the reconstruction. This dynamic procedure can be naturally applied to reconstruct a microstructure evolution process by continuously evolving a single microstructure according to a time-dependent correlation function. However, it is important to note that our dynamic reconstruction procedure can only be applied in the cases where a target microstructure or a series of auxiliary S_2 is given. If the only available structural information is a single S_2, our procedure cannot be applied and the standard YT method should be used instead.

The utility of our procedure is illustrated by successfully reconstructing systems containing well-separated particle phases near percolation such as the hard-sphere packing and SiC/Al composite, as well as a system containing bicontinuous interpenetrating phases such as the binary lead/tin alloy. These examples clearly indicate the validity and efficiency of the

dynamic reconstruction procedure in generating a wide class of complex microstructures and structural evolution.

Although the two-point correlation function S_2 is employed as the input structural information for dynamic reconstruction, this procedure can be easily generalized to utilize other limited morphological information. For example, limited-angle projections obtained via *in situ* x-ray tomography can be used to reconstruct the continuous evolution of a single material due to external stimuli [47]. This will significantly reduce the cost to separately reconstruct individual material microstructures at discrete time points.

ACKNOWLEDGMENTS

S.C., H.L., and Y.J. thank Arizona State University for the generous start-up funds. This work is partially support by the Division of Materials Research at National Science Foundation under Grant No. DMR-1305119.

[1] S. Torquato, J. Stat. Phys. **45**, 843 (1986).
[2] S. Torquato, *Random Heterogeneous Materials: Microstructure and Macroscopic Properties*, Vol. 16 (Springer Science & Business Media, Berlin, 2002).
[3] M. Sahimi, *Heterogeneous Materials I: Linear Transport and Optical Properties*, Vol. 1 (Springer Science & Business Media, Berlin, 2003).
[4] A. C. Kak and M. Slaney, *Principles of Computerized Tomographic Imaging*, Vol. 33 (SIAM, Philadelphia, 1988), xii.
[5] D. Brandon and W. D. Kaplan, *Microstructural Characterization of Materials* (John Wiley & Sons, New York, 2013).
[6] G. T. Herman, *Fundamentals of Computerized Tomography: Image Reconstruction from Projections* (Springer Science & Business Media, Berlin, 2009).
[7] J. Baruchel, P. Bleuet, A. Bravin, P. Coan, E. Lima, A. Madsen, W. Ludwig, P. Pernot, and J. Susini, Comptes Rendus Physique **9**, 624 (2008).
[8] C. J. Gommes, J. Appl. Crystal. **46**, 493 (2013).
[9] D. Alaimo, D. Hermida Merino, B. Grignard, W. Bras, C. Jérôme, A. Debuigne, and C. J. Gommes, J. Phys. Chem. B **119**, 1706 (2015).
[10] A. P. Roberts, Phys. Rev. E **56**, 3203 (1997).
[11] C. L. Y. Yeong and S. Torquato, Phys. Rev. E **57**, 495 (1998).
[12] C. L. Y. Yeong and S. Torquato, Phys. Rev. E **58**, 224 (1998).
[13] D. Fullwood, S. Kalidindi, S. Niezgoda, A. Fast, and N. Hampson, Mater. Sci. Eng. A **494**, 68 (2008).
[14] D. T. Fullwood, S. R. Niezgoda, and S. R. Kalidindi, Acta Mater. **56**, 942 (2008).
[15] A. Hajizadeh, A. Safekordi, and F. A. Farhadpour, Adv. Water Res. **34**, 1256 (2011).
[16] P. Tahmasebi and M. Sahimi, Phys. Rev. Lett. **110**, 078002 (2013).
[17] S. Torquato, Appl. Mech. Rev. **44**, 37 (1991).
[18] S. Torquato, Phys. Rev. Lett. **79**, 681 (1997).
[19] D. Pham and S. Torquato, J. Appl. Phys. **94**, 6591 (2003).
[20] B. Lu and S. Torquato, Phys. Rev. A **45**, 922 (1992).
[21] S. Torquato and M. Avellaneda, J. Chem. Phys. **95**, 6477 (1991).
[22] S. Torquato, J. Beasley, and Y. Chiew, J. Chem. Phys. **88**, 6540 (1988).
[23] S. Torquato, J. Chem. Phys. **85**, 4622 (1986).
[24] M. E. Frary and C. A. Schuh, Phys. Rev. E **76**, 041108 (2007).
[25] S. E. Wilding and D. T. Fullwood, Comput. Mater. Sci. **50**, 2262 (2011).
[26] J. Basinger, E. Homer, D. Fullwood, and B. Adams, Scripta Mater. **53**, 959 (2005).
[27] Y. Gueguen and J. Dienes, Math. Geology **21**, 1 (1989).
[28] N. Sheehan and S. Torquato, J. Appl. Phys. **89**, 53 (2001).
[29] M. G. Rozman and M. Utz, Phys. Rev. Lett. **89**, 135501 (2002).
[30] Y. Jiao, F. H. Stillinger, and S. Torquato, Proc. Natl. Acad. Sci. USA **106**, 17634 (2009).
[31] T. Tang, Q. Teng, X. He, and D. Luo, J. Microscopy **234**, 262 (2009).
[32] L. M. Pant, S. K. Mitra, and M. Secanell, Phys. Rev. E **90**, 023306 (2014).
[33] Y. Jiao, F. H. Stillinger, and S. Torquato, Phys. Rev. E **76**, 031110 (2007).
[34] Y. Jiao, F. H. Stillinger, and S. Torquato, Phys. Rev. E **77**, 031135 (2008).
[35] Y. Jiao, E. Padilla, and N. Chawla, Acta Mater. **61**, 3370 (2013).
[36] S. S. Singh, J. J. Williams, Y. Jiao, and N. Chawla, Metal. Mater. Trans. A **43**, 4470 (2012).
[37] K. M. Gerke, M. V. Karsanina, R. V. Vasilyev, and D. Mallants, Europhys. Lett. **106**, 66002 (2014).
[38] Y. Jiao and N. Chawla, J. Appl. Phys. **115**, 093511 (2014).
[39] Y. Jiao, F. H. Stillinger, and S. Torquato, Phys. Rev. E **82**, 011106 (2010).
[40] C. J. Gommes, Y. Jiao, and S. Torquato, Phys. Rev. Lett. **108**, 080601 (2012).
[41] C. E. Zachary and S. Torquato, Phys. Rev. E **84**, 056102 (2011).
[42] E.-Y. Guo, N. Chawla, T. Jing, S. Torquato, and Y. Jiao, Mater. Character. **89**, 33 (2014).
[43] S. Kirkpatrick, C. D. Gelatt, and M. P. Vecchi, Science **220**, 671 (1983).
[44] Y. Jiao, F. H. Stillinger, and S. Torquato, J. Appl. Phys. **109**, 013508 (2011).
[45] N. Chawla, V. Ganesh, and B. Wunsch, Scripta Mater. **51**, 161 (2004).
[46] S. Torquato and Y. Jiao, Nature **460**, 876 (2009).
[47] H. Li, N. Chawla, and Y. Jiao, Scripta Mater. **86**, 48 (2014).